


RESEARCH ARTICLE

Beyond life: Exploring hemodynamic patterns in postmortem mice brains

Anton Sdobnov¹ | Vassiliy Tsytsarev² | Gennadi Piavchenko³  |
Alexander Bykov¹ | Igor Meglinski³ 

¹Optoelectronics and Measurement Techniques, University of Oulu, Oulu, Finland

²Department of Neurobiology, University of Maryland School of Medicine, Baltimore, Maryland, USA

³Department of Human Anatomy and Histology, Institute of Clinical Medicine N.V. Sklifosovsky, I.M. Sechenov First Moscow State Medical University, Moscow, Russia

Correspondence

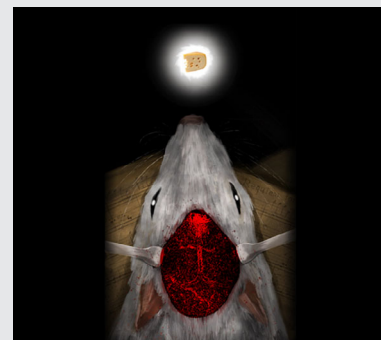
Igor Meglinski, College of Engineering and Physical Sciences, Aston University, Birmingham B4 7ET, UK.
Email: i.meglinski@aston.ac.uk

Funding information

COST (European Cooperation in Science and Technology); Royal Society; Russian Science Foundation, Grant/Award Number: 22-65-00096; European Union's Horizon 2020 research and innovation programme, Grant/Award Number: 863214

Abstract

We utilize Laser Speckle Contrast Imaging (LSCI) for visualizing cerebral blood flow in mice during and post-cardiac arrest. Analyzing LSCI images, we noted temporal blood flow variations across the brain surface for hours postmortem. Fast Fourier Transform (FFT) analysis depicted blood flow and microcirculation decay post-death. Continuous Wavelet Transform (CWT) identified potential cerebral hemodynamic synchronization patterns. Additionally, non-negative matrix factorization (NMF) with four components segmented LSCI images, revealing structural subcomponent alterations over time. This integrated approach of LSCI, FFT, CWT, and NMF offers a comprehensive tool for studying cerebral blood flow dynamics, metaphorically capturing the 'end of the tunnel' experience. Results showed primary postmortem hemodynamic activity in the olfactory bulbs, followed by blood microflow relocations between somatosensory and visual cortical regions via the superior sagittal sinus. This method opens new avenues for exploring these phenomena, potentially linking neuroscientific insights with mysteries surrounding consciousness and perception at life's end.



KEYWORDS

blood flow, brain microcirculation, continuous wavelet transform, laser speckle contrast, non-negative matrix factorization, postmortem

1 | INTRODUCTION

The enigmatic experience of a 'light at the end of the tunnel', reported throughout history, has long intrigued both the scientific community and the public.

Neurophysiological investigations following cardiac arrest have uncovered organized electrical brain signals in rats [1] and distinctive slow-wave patterns in human electroencephalograms (EEG) readings [2], phenomena often termed the 'wave of death'. These findings only

This is an open access article under the terms of the [Creative Commons Attribution](https://creativecommons.org/licenses/by/4.0/) License, which permits use, distribution and reproduction in any medium, provided the original work is properly cited.

© 2024 The Authors. *Journal of Biophotonics* published by Wiley-VCH GmbH.

begin to unravel the complexities of brain activity during and after the death process [3], with electrical activities akin to those seen in deep sleep observed to persist even 10 min following the clinical declaration of [4]. Furthermore, recent revelations suggest the possibility of a post-mortem revival in brain microcirculation and cellular functions, occurring several hours after death [5]. In addition to these observations, recent years have seen increased focus on neurovascular changes during hypoxia in the terminal stage. Studies analyzing EEG data of dying patients before and after the cessation of mechanical ventilation [6, 7] have identified stimulation of gamma activity by global hypoxia in some cases. However, the underlying mechanisms and physiological significance of these observations, including those related to cerebral hemodynamics postmortem, remain largely unclear [8, 9]. This context frames our study's aim to explore further and bridge the gap between these initial observations and a deeper understanding of postmortem brain activity.

While the causal relationship between neural activity and hemodynamics is beyond doubt, the deeper mechanisms underlying this link, especially postmortem, remain a subject of ongoing research [10–13]. Studies using dynamic light scattering (DLS)-based approach and direct optical vascular imaging techniques have uncovered randomized blood microflows in various tissues of small animals for hours after death [14]. Furthermore, separate assessments of cerebral blood flow impairments caused by cardiac and respiratory arrest using multi-modal diagnostic tools have been conducted [15]. These studies reveal that cerebral hemodynamic alterations, similar to electrical brain activities, persist for several hours following respiratory arrest or cessation of blood flow. However, despite the accumulation of data, the precise mechanisms driving these cerebral hemodynamic variations and their structural organization postmortem are still not fully understood. This gap in knowledge is particularly notable when considering the substantial anatomical differences between the rodent and human brain, suggesting that the sequence of irreversible changes following oxygen deprivation may vary significantly across species.

DLS-based techniques, including LSCI, play a crucial role in brain imaging due to their unique ability to non-invasively monitor and analyze cerebral blood flow and microcirculation in real-time. These techniques are particularly significant for understanding neurovascular dynamics, aiding in the exploration of various physiological and pathological conditions within the brain [16]. LSCI, as a specific DLS-based approach, stands out for its high temporal resolution, which allows for the observation of rapid real-time hemodynamic changes, and its ease of use, making it accessible for both clinical and research settings. LSCI is a valuable tool for real-time,

non-invasive monitoring of cerebral blood flow, particularly during surgeries [17], and its capability to quantitatively analyze blood flow dynamics plays an invaluable role in advancing our understanding of cerebral hemodynamics, offering a comprehensive perspective on brain function and health [18]. However, due to the complexity of the data it generates, additional statistical analysis and segmentation are often required to accurately quantify blood flow, enhance image clarity, and ensure the images are useful for medical decision-making [19].

Statistical analysis, including techniques like wavelet transform, and spectral analysis methods such as fast Fourier transform (FFT), enhance the interpretability of LSCI data by decomposing complex blood flow signals into simpler components [20–22]. This helps in identifying specific physiological phenomena or vascular responses, such as those occurring during reactive hyperemia. While FFT is excellent for identifying the overall frequency content of a signal, wavelet analysis [22] excels in analyzing signals where frequency components vary over time, making it a more versatile tool for detailed time–frequency analysis, especially for non-stationary signals like those often encountered in LSCI.

In fact, non-negative matrix factorization (NMF) [23] offers certain advantages compared to FFT and wavelet transform, particularly in the context of analyzing complex data like LSCI images. NMF tends to produce a part-based representation, where each component reflects a part or a feature of the data. This is particularly useful in image analysis, as it can lead to the identification of distinct patterns or regions within the image, which might correspond to specific physiological or anatomical structures. NMF's strength lies in its ability to decompose data into non-negative, interpretable components, making it particularly useful for image analysis and feature extraction. This contrasts with FFT and wavelet transform, which are more focused on signal frequency and time–frequency analysis. While all FFT, wavelet analysis and NMF are valuable for the LSCI data analysis, their applications and focus in analyzing LSCI are different. FFT and wavelet analysis are particularly suited for examining temporal and spatial patterns in dynamic signals like blood flow, while NMF is more aligned with decomposing data into interpretable, static components.

In the current study, we apply the Laser Speckle Contrast Imaging (LSCI) approach, specifically developed for transcranial optical vascular imaging (nTOVI) [24], to investigate cerebral hemodynamic alterations following cardiac cessation. To enhance clarity, the obtained LSCI images were processed using both FFT [25] and Continuous Wavelet Transform (CWT), specifically employing the Mexican hat wavelet [26], as well as the NMF analytical approach [27]. More specifically, we introduce the application of NMF

not only for segmenting individual LSCI images into meaningful components but also for analyzing a series of LSCI images over time, thereby revealing temporal alterations in structural subcomponents.

2 | MATERIALS AND METHODS

2.1 | LSCI experiment

In recent years, LSCI has emerged in the field of neurobiology as a method for functional brain mapping [16, 17]. This method is based on analyzing the blurring effect of the speckle pattern. When a physically inhomogeneous surface is illuminated by a coherent light, photodetectors can collect information about the numerous speckles created by the interference of coherent light. If the surface scanning and photodetector properties offer sufficient speed, this method can depict the functional features of the brain at each point in the image. Typically, in biological and medical research, a laser of the far red or near-infrared part of the spectrum is employed, which allows for deeper penetration of photons into the cortical tissue.

The developed LSCI experimental system is a portable and effective non-invasive imaging technique. It is widely used for monitoring functional and morphological changes in blood perfusion, as well as relative blood flow variations in the brain [28], tumors [29], and skin tissues in vivo [30, 31]. This setup has been employed for visualizing postmortem hemodynamics in the mouse brain. A 3 mW laser diode with an output wavelength of 808 nm (LDM808/3LJ, Roithner Lasertechnik GmbH, Austria) served as the light source. The beam from the laser diode passed through a diffuser (ED1-C20, Thorlabs, USA) to ensure uniform distribution of laser radiation over the observed brain area. Image acquisition was performed using a CMOS camera (DCC3240M, 1280 × 1024 resolution, pixel size 6.7 μm, Thorlabs, USA) combined with a 12 mm F1.4 objective lens (Kenko Tokina Co., Ltd., Japan). The camera captured raw speckle patterns with an exposure time of 10 ms. A series of 100 consecutive raw speckle images were obtained every 10 s during the experiment for further processing. Each series of images was then processed using a custom-developed temporal speckle contrast algorithm [5] based on MATLABr2019b software, assisted by a standard Fiji/ImageJ plugin [32]. This approach has been successfully used in transcranial vascular imaging [24] and cross-validated using fluorescent intravital microscopy [28], among other studies [33].

The measurement of pulse rate (in beats per minute or bpm) and oxygen saturation (SpO₂) was conducted using an MD300M-V pulse oximeter (ChoiceMMED,

China). The system is capable of assessing and recording these parameters every 4 s with the minimal measured pulse rate is 30 bpm.

2.2 | LSCI data processing

The quantitative analysis in LSCI typically involves calculating the speckle contrast ratio (K), which quantifies the variation in the speckle pattern. The speckle contrast ratio is defined as the ratio of the standard deviation (σ) of the intensity in the speckle pattern to its mean intensity ($\langle I \rangle$) within a region of interest. Mathematically, the speckle contrast ratio K is expressed as:

$$K = \frac{\sigma}{\langle I \rangle}. \quad (1)$$

A higher K value indicates less blurring, corresponding to slower blood flow, while a lower K value indicates more blurring, corresponding to faster blood flow. The commonly used model is based on the temporal statistics of speckle intensity fluctuations [16], leading to an expression that connects the speckle contrast K to the exposure time (T) of the camera, the mean velocity of scatterers (blood cells) in the illuminated volume, and the speckle size. The simplified relation under certain assumptions (such as uniform velocity of scatterers and fully developed speckle) is expressed as [34]:

$$K = \beta^{0.5} \left\{ \frac{\tau_c}{T} + \frac{\tau_c^2}{2T^2} \left[\exp\left(\frac{2T}{\tau_c}\right) - 1 \right] \right\}^{0.5}, \quad (2)$$

where τ_c is the decorrelation time, related to the inverse of the mean velocity of the scatterers and β represents the aperture parameter, conceptually understood as the geometry-specific contrast relative to the measurement setup, or the degree of coherence of the detected signal. This equation is used in a context to provide an understanding of how speckle contrast is related to the motion (e.g., blood flow). In fact, detailed analysis requires more sophisticated models that consider various factors like multiple scattering, speckle geometry, and the spatial-temporal distribution of scatterer velocities and other [16].

In practice speckle contrast parameter is typically calculated using either spatial approach (using sliding window) or temporal approach (statistics calculated in each pixel of images sequence) [16, 35]. The spatial approach calculates speckle contrast by analyzing the intensity variations across a spatial region in a single image. A sliding window moves across the image, and for each position of

the window, the speckle contrast is calculated using the intensities of the pixels within that window. The temporal approach calculates speckle contrast by analyzing the intensity variation of each pixel across a sequence of images over time. For each pixel, the speckle contrast is determined using its intensity values across the time series. The choice between spatial and temporal approaches depends on the specific requirements of the study, including the need for real-time imaging, the importance of spatial versus temporal resolution, and the available imaging equipment. Temporal analysis requires a series of images and thus more data storage and potentially more complex post-processing, but it provides valuable insights into how blood flow changes over time. In contrast, spatial analysis provides a snapshot of blood flow distribution across an area at a given time, which can be sufficient for many applications and is computationally less demanding.

In current study, the speckle statistics has been calculated within sliding window with the size of 5×5 pixels over raw speckle images sequence obtained from a CCD camera. Further, FFT [25] and Continuous CWT employing the Mexican hat wavelet [26] were applied to obtained time sequence of speckle contrast images. Finally, NMF approach has been also applied for calculated speckle contrast images [27]. NMF is especially useful for non-negative data such as functional images, particularly speckle contrast images, where value in each pixel is between 0 and 1.

In general, the measured data matrix $V = [V_1, V_2, \dots, V_m]$ consisting of M measurements of N non-negative scalar variables is approximated using factorization: $V \approx WH$, where matrix $W = [W_1, W_2, \dots, W_m]$ with $m \times k$ dimension and $H = [H_1, H_2, \dots, H_m]$ with $k \times n$ dimensions. The decision on which value of k components should be used in most cases depends on inequality $k \ll \min(m, n)$. In this case, WH can be considered as a compressed form of the data in V . After NMF application, the data in H ($k \times m$ elements) can be considered as transformed database with lower number of features (k), than the original database V . Here, we implemented unsupervised machine learning NMF algorithm using python programming language for assessment of mouse brain vasculature after death. For NMF, the $k = 4$ has been used.

2.3 | Small animal preparation

CD1 nude female mice, aged 6–8 weeks and obtained from Envigo, were used in the study. All animal studies received approval from Sechenov University Local Ethical Committee (protocol No. 23-22 dated November 17, 2022). The animals were anesthetized with a combination of 10 mg/100 mg/kg ketamine (Vetoquinol, Lure,

France) and xylazine (Eurovet Animal Health, Bladel, The Netherlands) through intraperitoneal injection. Previous research has shown that the mouse brain's vasculature can be clearly observed using LSCI through the intact skull. However, skin removal is still necessary for optimal visibility. Therefore, following the administration of general anesthetics, an initial incision was made, and the skin over the frontal, temporal, occipital, and parietal regions was removed by blunt dissection. This procedure was conducted to enhance the visibility of the brain's blood vessels and minimize static scattering that affects ergodic conditions. The exposed area of interest was constantly moistened with saline. Subsequently, the animal was placed in the imaging setup on a specialized mouse holder, with measurements performed at room temperature (25°C). To register post-mortem brain hemodynamic activities, the animal was euthanized using a barbiturate overdose. The raw speckle images were captured within 60 min after the injection.

3 | RESULTS AND DISCUSSION

The obtained results are presented in Figure 1. For the better clarity, the background area outside brain has been colored in gray.

The time series of LSCI images reveals temporal variations in the spatial distribution of blood flow across the brain surface, as illustrated in Figure 1, line 1. Decomposition of these images using FFT captures the decay of oscillations in blood flow and microcirculation following the animal's death, shown in Figure 1, line 2. Considering the non-stationary nature of the recorded LSCI image set, and the variability of its statistical properties over time, we applied CWT to investigate the emergence of cerebral hemodynamic patterns indicating spatial and/or temporal synchronization across the brain surface (see Figure 1, line 3). Additionally, we employed NMF for segmenting LSCI images, which aids in identifying interpretable relationships within distinct, demarcated microstructural patterns for functional evaluation, as detailed in Figure 1, line 4. To effectively characterize postmortem cerebral hemodynamics and delineate its features, we selected four NMF components, balancing stability and accuracy as referenced in previous studies [27]. These components represent distinct patterns of microstructural variance in cerebral blood microcirculation, and their temporal analysis offers profound insights into the complexity and heterogeneity of hemodynamic localization, both spatially and temporally. The NMF approach thus facilitates the identification of distinct microstructural components, enhancing our understanding of hemodynamic pattern formation in specific cortical zones and their functional implications. The color-coded representations of these four NMF

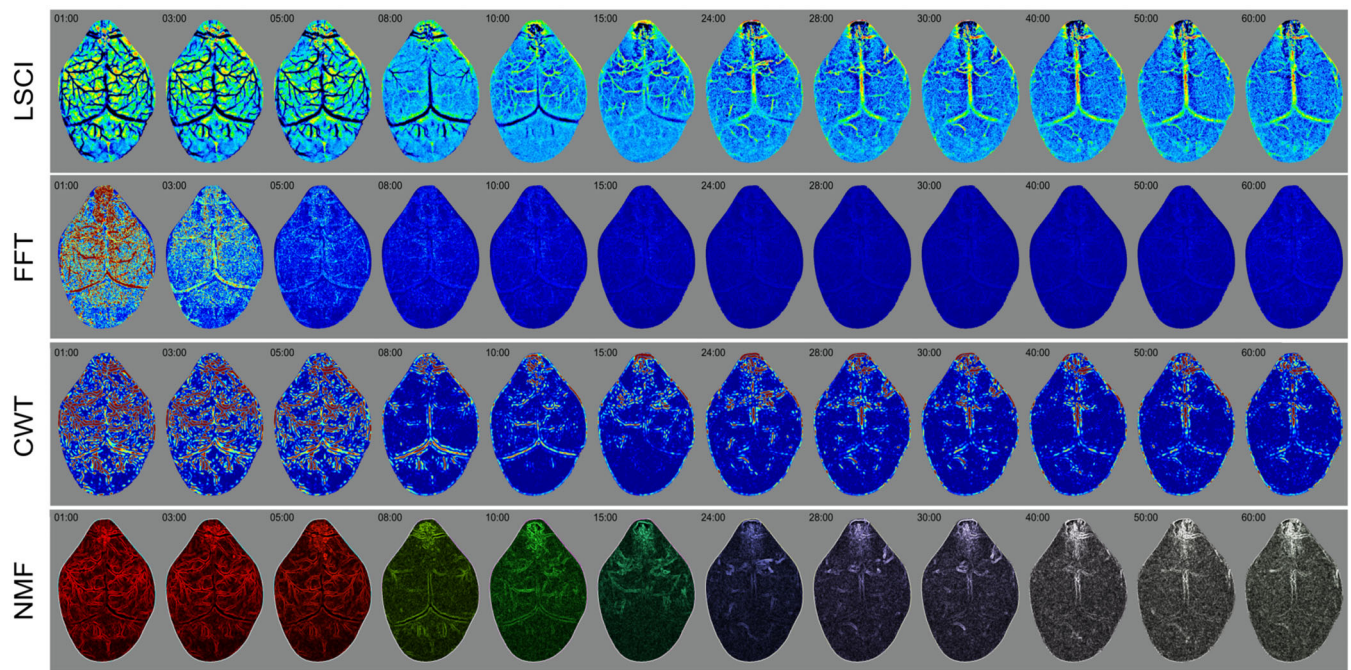
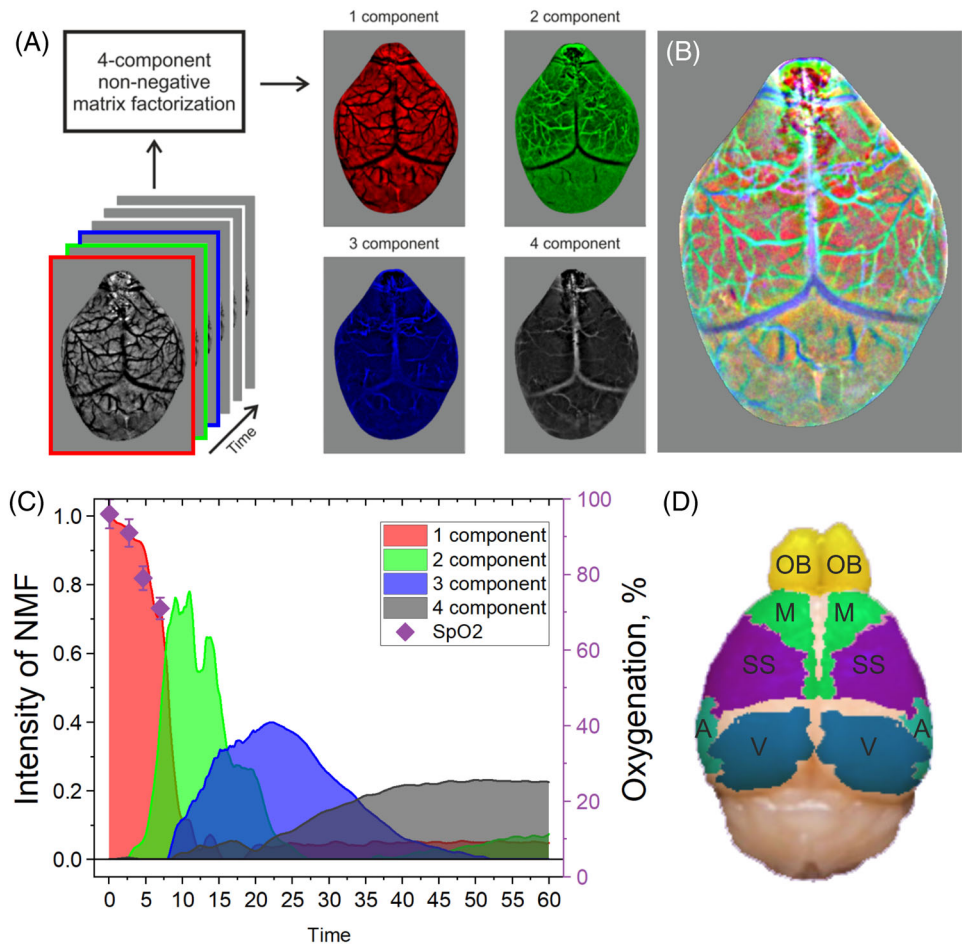


FIGURE 1 The color-coded images of mouse brain obtained, respectively, by LSCI (first line), FFT (second line), CWT (third line) and NMF (forth line) at different time intervals after the cardiac arrest. Video S1 shows full time series of LSCI, FFT, CWT, and NMF. Time intervals are selected according NMF component analysis discussed below.

FIGURE 2 (A) Time series of LSCI images and corresponding color-coded images of the four NMF components (red, green, blue, and gray, respectively); (B) Merged image of the four color-coded NMF components. Video S1d shows the dynamics of the spatial distribution of the merged four NMF components; (C) Weighted contribution of the NMF components in the merged distribution over time; \blacklozenge shows oxygen saturation (SpO₂) referring to the right axis for the corresponding values. (D) Corresponding map of the main areas of neuronal activity in the mouse brain: A, auditory cortex; M, motor cortex; OB, olfactory bulb; SS, somatosensory cortex; V, visual cortex. Scale bar equals 1 mm.



components and their combined weighted spatial distribution over time are presented in Figure 2.

The time series of LSCI images of the mouse brain obtained postmortem, as well as those processed using FFT, CWT, and NMF, show that the distribution of cerebral blood flow is highly non-homogeneous, with pronounced spatial and temporal hemodynamic localizations (see Figures 1 and 2, and associated Video S1). In line with previous studies that demonstrate a strong spatial relationship between hemodynamic changes and neural activity [36–38], also known as neurovascular coupling [39], the identified localizations of cerebral blood flow and blood microcirculation have been compared with a confirmed anatomical template and corresponding neuroanatomical domains [40]. The results obtained through LSCI, FFT, CWT, and NMF (see Figures 1 and 2, and Video S1) clearly reveal predominant hemodynamic localization in the olfactory bulbs. Additionally, successive alternate relocations of postmortem systolic blood micro-flow localizations, facilitated by the superior sagittal sinus, are observed between the somatosensory and visual cortical regions. Along with the results obtained by FFT and CWT (see Figure 1 and Video S1), NMF identifies temporal alterations of structural subcomponents, which exhibit a coherent evolution without being constrained by anatomical delineations (see Figure 2 and Video S1).

In current study, the use of FFT is pivotal in elucidating the decay patterns of blood flow and microcirculation post-mortem. Unlike other analytical methods that offer temporal or spatial insights, FFT provides a unique advantage in identifying and quantifying the frequency content of dynamic signals over time. This capability is particularly crucial in present studies, where understanding the frequency domain representation of cerebral hemodynamics offers significant insights into the physiological processes occurring during and after cardiac arrest. By employing FFT, we are able to decompose complex blood flow signals into their constituent frequencies, revealing underlying patterns of hemodynamic activity that are not readily apparent in the time domain. This analysis facilitated a clearer understanding of the oscillatory nature of post-mortem blood flow (see Figure 1 and Video S1), enabling to quantify the gradual reduction in hemodynamic activity and its correlation with the cessation of cardiac function.

Furthermore, FFT's ability to isolate specific frequency components from the overall signal allowing to discern subtle shifts in the hemodynamic response that indicates residual neurovascular coupling or the initiation of post-mortem metabolic processes. These insights are invaluable in advancing a comprehension of the cerebral blood flow dynamics during the critical transition

from life to post-mortem states, shedding light on the complex interplay between neural activity and vascular response in the absence of cardiac function.

In addition to FFT, in the intricate exploration of cerebral hemodynamics, particularly in postmortem conditions, our research harnesses the CWT to uncover and analyze potential cerebral hemodynamic synchronization patterns (see Figure 1). Unlike traditional FFT methods, which excel in identifying the overall frequency content but lack the temporal localization of these frequencies, CWT stands out for its exceptional ability to provide a detailed time-frequency representation of non-stationary signals. This attribute of CWT is invaluable in our study, as it allows for the nuanced detection and characterization of transient hemodynamic events and their synchronization across different brain regions over time (see Figure 1 and Video S1).

The employment of CWT, specifically utilizing the Mexican hat wavelet, facilitates a fine-grained analysis of the temporal evolution of cerebral blood flow dynamics. This is pivotal for identifying the onset, duration, and spatial distribution of hemodynamic patterns that emerge following cardiac arrest. By enabling the observation of these dynamic patterns at various scales and moments, CWT significantly enhances our understanding of the underlying physiological processes driving postmortem cerebral blood flow.

Moreover, the capability of CWT to dissect the complex LSCI data into meaningful temporal and spatial components aids in revealing the intricacies of neurovascular coupling and its persistence even in the absence of cardiac function. This deeper insight into cerebral hemodynamics is crucial for unraveling the physiological significance of observed neurovascular changes during hypoxia in the terminal stage, thus bridging a critical gap in the current understanding of postmortem brain activity.

The selected NMF components are used to identify and evaluate the LSCI images in terms of their spatial variations in postmortem cerebral hemodynamics over time (see Figures 1 and 2, and Video S1). In the first 8 min following death, hemodynamic activity is predominantly observed in the cerebral cortex, and olfactory bulbs, visual, as well as in the cerebellum. The 1st NMF component, representing a rapid decrease in hemodynamic intensity during the initial period followed by subsequent redistribution to the largest venous sinuses, aligns with the observed decrease in oxygen saturation (SpO₂) from 97% to 71% within the first 8 min (see Figure 2). This correlation between the 1st component and the significant drop in oxygen saturation underscores its relevance in capturing physiological changes during this timeframe. However, longer measurements were not

feasible, as the pulse oximeter's technical limitations restrict its ability to accurately measure oxygen saturation levels below a minimum of 70%. The 2nd NMF component, appearing from the 4th to approximately the 25th minute, represents low-frequency pulsating blood flow in the sagittal sinus. The 3rd NMF component, active between 8 and 39 min, indicates further hemodynamic redistribution in specific cortical areas between arterial and venous vessels. Finally, the 4th NMF component, emerging around the 25th minute, is characterized by periodic hemodynamic relocations via the superior sagittal sinus.

The analysis of postmortem cerebral hemodynamics using LSCI, complemented by techniques such as NMF, FFT, and CWT, sheds light on the intricately complex process by which different parts of the brain cease to function following the cessation of blood circulation and oxygen supply. Although there is no definitive consensus yet, our observations contribute to the ongoing research in understanding this sequence. Preliminary findings suggest a potential order of impact: primary sensory areas, vital for basic sensory perceptions, are likely affected first due to their increased sensitivity to oxygen deprivation, as evidenced by the dominant hemodynamic activity observed in these areas immediately postmortem. This is followed by the impairment of higher-order sensory and motor areas, responsible for complex processing and coordination, which aligns with the redistribution of hemodynamic intensity detected in these regions. Association areas, crucial for higher cognitive functions, initially show resilience but gradually succumb to hypoxia, a pattern that can be traced through the temporal alterations identified by the NMF components. Ultimately, the frontal lobes, integral to executive functions, are among the last to be impacted, which correlates with the later stages of hemodynamic changes observed. It is important to recognize, however, that this sequence is not absolute and may vary across different species and under various conditions.

During the experiment, we observed a sequence of biological and physical phenomena related to brain activity and death, phenomena that have been extensively studied in prior research. Cardiac arrest, if not promptly compensated for, inevitably leads to the asphyxiation of all body organs, including the brain. Brain asphyxia lasting more than a few minutes typically results in brain death, a condition often used as a legal indicator of death. However, the definition of brain death is not universally accepted due to the variability in brain function cessation; different brain regions can cease functioning at different times. Brain death is frequently defined as the cessation of function in all parts of the brain, including the brain stem, yet cases exist where the brain stem

remains active, enabling spontaneous breathing even when the rest of the brain has ceased functioning. In such cases, only life support equipment can maintain respiration. Distinguishing between brain death, coma, and chronic vegetative states presents a clinical challenge, as indicated by Bugge et al. [41]. An absence of electrical activity, which can be detected through an EEG, may occur not only in brain death but also in deep anesthesia or during cardiac arrest.

Under conditions of oxygen deprivation, neurons lose their ability to generate action potentials, and glial cells also cease to function due to the failure of cell membranes to maintain the ionic balance between extra- and intracellular spaces. The resulting influx of ions causes a synchronous, massive depolarization of brain membranes, marking a transition from physiological to physical processes in the brain. Physically, this leads to brain swelling and compression of the capillaries, which can affect blood movement. This period is also characterized by a rapid transition from oxyhemoglobin to deoxyhemoglobin.

These intricate biological processes occurring during and after brain death can be precisely captured using optical brain imaging methods, including LSCI. It is essential to recognize that the optical correlates observed through LSCI will depict significantly different processes before and after the onset of brain death. Currently, numerous questions about the biological processes associated with brain death remain unanswered. Notably, brain activity has been observed 10 min after the cessation of the heartbeat and the loss of all brain reflexes [4]. Additionally, experimental evidence suggests that conventional understanding of the rapid cessation of neuronal activity and irreversible changes in cellular structure post-brain death may need reconsideration. For instance, studies have shown that cellular functions of pig brain neurons can be restored hours after death. In one such study, 4 h postmortem, a synthetic fluid called BrainEx, mimicking blood, was circulated through the pig brain [5]. This infusion of BrainEx was found to restore normal cellular metabolism, such as glucose utilization and ATP synthesis, in neurons and other brain cells, while preserving the structural integrity of these cells. Moreover, electrical stimulation led to the generation of action potentials in individual neurons [5].

However, the neuronal spikes observed were scattered and unsynchronized, indicating the absence of neural network functionality and, consequently, consciousness [42]. This finding aligns with research showing that mitochondria from the mammalian brain remain viable for several hours postmortem [43]. As a result, the idea that, under certain conditions, molecular and cellular functions in the mammalian brain might retain a

partial capacity for recovery even after a prolonged post-mortem interval appears reasonable [5]. Hence, current experimental and clinical data suggest that microcirculation and specific molecular and cellular functions in the brains of large mammals can be restored after brain death. It is increasingly evident that the molecular and cellular deterioration of the brain following circulatory arrest may be a more protracted process than previously believed, suggesting that the mammalian brain might possess a greater capacity for metabolic and neurophysiological stability under hypoxic conditions than is currently acknowledged [5]. While it may be somewhat premature to draw definitive conclusions about the process of neurovascular coupling in various brain regions during the terminal stage of hypoxia, the technique we have presented in this study marks a significant step forward in exploring this complex phenomenon.

These data will logically be compared with the clinical results of Emergency Preservation and Resuscitation (EPR) [44]. EPR technique was developed to use hypothermia to gain time during long-term cerebral hypoxia and allow delayed resuscitation. Also, animal studies have shown that cooling the body can cause circulatory arrest for up to 2 h, followed by normal neurological recovery. This provides additional evidence that the process of irreversible destruction of neurons and astrocytes after cessation of blood supply to the brain may be longer than is commonly believed [44].

4 | SUMMARY AND CONCLUSIONS

In conclusion, our pioneering application of NMF for both segmenting individual LSCI images and analyzing temporal series of these images has led to revealing significant temporal alterations in structural subcomponents. By employing a novel, integrated approach that combines LSCI, FFT, CWT, and NMF, we have succeeded in comprehensively analyzing cerebral blood flow dynamics in mice. This advancement not only contributes to our understanding of cerebral hemodynamics but also opens up new possibilities for exploring dynamic changes in brain function and pathology. This multifaceted methodology allowed us to metaphorically capture the 'end of the tunnel' experience, revealing intricate details of postmortem mice's neural activity. The obtained results indicated a primary localization of hemodynamic activity in the olfactory bulbs after death, suggesting a sustained sensory perception related to smell. This was followed by minor, but distinct, successive relocations of blood microflows between the somatosensory and visual cortical regions, facilitated by the superior sagittal sinus.

The adoption of this integrated approach has proven instrumental in elucidating the complex interplay of sensory processing and blood flow dynamics in the brain at the end of life. It provides a robust framework for interpreting the subtle shifts in neural activity and offers a comprehensive tool for visualizing and understanding these phenomena. This innovative methodological convergence opens new avenues for exploration into cerebral hemodynamics and sensory experiences postmortem. It holds the potential to bridge significant gaps in our neuroscientific understanding, particularly regarding the enigmatic aspects of consciousness and perception at life's end. The insights gained from this study not only enhance our comprehension of cerebral physiology in mice but also lay the groundwork for future research that could extrapolate these findings to broader biological and philosophical contexts. An innovative artistic installation visually and conceptually illustrates what mice arguably perceive at the end of the tunnel (Figure 3). It combines the temporal variations of postmortem hemodynamic activities in the mouse brain with an artistic representation of this experience. The installation depicts the 'end of the tunnel' as a faintly flickering light in twilight, accompanied by the sensation of soft puffs of air and a strong olfactory sensation, most likely akin to cheese. This artistic and scientific fusion in Figure 3 not only conveys our findings in a visually compelling manner but also provides a unique perspective on the sensory experiences of mice at life's end. It opens new avenues for exploring these phenomena, potentially bridging the gap between neuroscientific understanding and the longstanding mysteries surrounding consciousness and perception at the end of life. The insights gained from this study enhance our understanding of cerebral physiology and sensory processing in mice, paving the way for further research into these complex and fascinating aspects of neural activity. In addition, the methodology developed in this study holds promise for broader applications in biomedical research, potentially paving the way for improved diagnostic tools and therapeutic strategies in neurology and various other medical disciplines.

It should be also pointed out that the LSCI application in the experimental paradigm we used is only one way to study the problem of neurovascular coupling in the terminal state of the brain. Other functional brain imaging methods, including multimodal approaches also can be very effective. Various imaging techniques, including fMRI, will definitely be widely used in terminal brain studies in animal models. However, fMRI can also bring unique insights from clinical practice. Thus, after an elderly patient suddenly died during an fMRI scan for reasons unrelated to the scan, researchers obtained unique data on brain activity at the very end of his life [8].



FIGURE 3 Artistic interpretation of mice's perceptual experience at life's end. This illustration conceptualizes the 'end of the tunnel' vision for mice, as a blend of dim, flickering light reminiscent of twilight, coupled with sensations of gentle air currents and a distinct olfactory impression, likely resembling cheese. Video S2 complements this illustration by showcasing the temporal variations in postmortem hemodynamic activities within the mouse brain, integrated with this artistic representation of sensory experiences at the end of life.

Such studies, of course, are associated not only with methodological difficulties, but also require serious legal and ethical consideration. Definitely, fMRI can be used not only in clinical practice but also in animal models. However, despite being the gold standard of neuroimaging, this method has not only advantages but also disadvantages. Typically, when scanning the human brain, fMRI provides a spatial resolution of the order of one cube millimeter. This value can be significantly improved by increasing the power of the magnetic field, that is, through the use of more advanced scanners. It is also possible to reduce the volume of the part of the brain that is scanned. The third way to increase spatial resolution is to reduce temporal resolution. By combining these approaches, it is possible to achieve a voxel with an edge

length of about 100 μm . But even such spatial resolution will not make it possible to monitor local blood circulation in small vessels, since the diameter of brain capillaries can be about 10 μm . The temporal resolution of fMRI is typically in the range of about 1 s or slightly less. This is sufficient for functional mapping of the human brain, but completely insufficient for studying cerebral microcirculation. Thus, circulation of blood in the small blood vessels are beyond the spatial resolution of fMRI, but are perfectly imaged using LSCI. The capillaries' diameter allows optical methods not only to visualize the shape of the vessel, but also to determine a number of parameters of blood flow – first of all, the intensity of blood flow and oxygenation of hemoglobin at each moment of time. Besides that, in fMRI temporal resolution faces physical limitations, preventing the monitoring of rapid changes in cerebral blood flow and oxygenation, while optical methods, primarily LSCI, do not share these disadvantages. While optical imaging lacks the ability to perform 3D imaging, a multimodal approach involving combination of the optical methods and fMRI is feasible when working with animal models. Such multimodality undoubtedly holds significant promise, and we plan to continue research in this direction.

ACKNOWLEDGMENTS

The authors acknowledge help of Miss Tatian Koryashkina with the help of preparation of artistic installation presented in Figure 3.

FUNDING INFORMATION

Current study supported by COST Action CA21159 - Understanding interaction light - biological surfaces: possibility for new electronic materials and devices (PhoBioS), the European Union's Horizon 2020 research and innovation programme under grant agreement no. 863214—NEUROPA project and by the (UK), and the 'Perfect Match' Public Engagement grant. Authors also acknowledge partial support provided by the Russian Science Foundation—project no. 22-65-00096.

CONFLICT OF INTEREST STATEMENT

The authors declare no competing interests.

DATA AVAILABILITY STATEMENT

The data that support the findings of this study are available from the corresponding author upon reasonable request.

ORCID

Gennadi Piavchenko  <https://orcid.org/0000-0001-7782-3468>

Igor Meglinski  <https://orcid.org/0000-0002-7613-8191>

REFERENCES

- [1] J. Borjigin, U. Lee, T. Liu, D. Pal, S. Huff, D. Klarr, J. Sloboda, J. Hernandez, M. Wang, G. Mashour, *Proc. Natl. Acad. Sci. U. S. A.* **2013**, *110*, 14432.
- [2] C. Rijn, H. Krijnen, S. Menting-Hermeling, A. Coenen, *PLoS One* **2011**, *6*, e16514.
- [3] D. Auyong, S. Klein, T. Gan, A. Roche, D. Olson, A. Habib, *Anesth. Analg.* **2010**, *110*, 1428.
- [4] L. Norton, R. Gibson, T. Gofton, C. Benson, S. Dhanani, S. Shemie, L. Hornby, R. Ward, B. Young, *Can. J. Neurol. Sci.* **2017**, *44*, 139.
- [5] Z. Vrselja, S. Daniele, J. Silbereis, F. Talpo, Y. Morozov, A. Sousa, B. Tanaka, M. Skarica, M. Pletikos, N. Kaur, Z. W. Zhuang, Z. Liu, R. Alkawadri, A. J. Sinusas, S. R. Latham, S. G. Waxman, N. Sestan, *Nature* **2019**, *568*, 336.
- [6] D. Li, O. Mabrouk, T. Liu, F. Tian, G. Xu, S. Rengifo, S. Choi, A. Mathur, C. Crooks, R. Kennedy, M. M. Wang, H. Ghanbari, J. Borjigin, *Proc. Natl. Acad. Sci. U. S. A.* **2015**, *112*, E2073.
- [7] G. Xu, T. Mihaylova, D. Li, F. Tian, P. Farrehi, J. Parent, G. Mashour, M. Wang, J. Borjigin, *Proc. Natl. Acad. Sci. U. S. A.* **2023**, *120*, e2216268120.
- [8] R. Vicente, M. Rizzuto, C. Sarica, K. Yamamoto, M. Sadr, T. Khajuria, M. Fatehi, F. Moien-Afshari, C. Haw, R. Llinas, A. M. Lozano, J. S. Neimat, A. Zemmar, *Front. Aging Neurosci.* **2022**, *14*, 80.
- [9] N. Shlobin, J. Aru, R. Vicente, A. Zemmar, *Front. Aging Neurosci.* **2023**, *15*, 281.
- [10] D. Attwell, A. Buchan, S. Charpak, M. Lauritzen, B. MacVicar, E. Newman, *Nature* **2010**, *468*, 232.
- [11] Y. Ma, M. Shaik, M. Kozberg, S. Kim, J. Portes, D. Timerman, E. Hillman, *Proc. Natl. Acad. Sci. U. S. A.* **2016**, *113*, E8463.
- [12] D. Wu, X. Liu, K. Gadhoumi, Y. Pu, C. Hemphill, Z. Zhang, L. Liu, X. Hu, *J. Neural. Eng.* **2020**, *17*, 026006.
- [13] A. Bergel, E. Tiran, T. Deffieux, C. Demené, M. Tanter, I. Cohen, *Nat. Commun.* **2020**, *11*, 6193.
- [14] I. Meglinski, V. Kal'chenko, Y. Kuznetsov, B. Kuznik, V. Tuchin, *Dokl. Phys.* **2013**, *58*, 323.
- [15] G. Piavchenko, I. Kozlov, V. Dremin, D. Stavtsev, E. Seryogina, K. Kandurova, V. Shupletsov, K. Lapin, A. Alekseyev, S. Kuznetsov, A. Bykov, A. Dunaev, I. Meglinski, *J. Biophoton* **2021**, *14*, e202100216.
- [16] A. Sdobnov, G. Piavchenko, A. Bykov, I. Meglinski, *Las. Photon. Rev.* **2024**, *18*, 2300494.
- [17] A. Konovalov, V. Gadzhiagaev, F. Grebenev, D. Stavtsev, G. Piavchenko, A. Gerasimenko, D. Telyshev, I. Meglinski, S. Eliava, *World Neurosurg.* **2023**, *171*, 35.
- [18] S. Soloukey, A. Vincent, M. Smits, C. De Zeeuw, S. Koekkoek, C. Dirven, P. Kruizinga, *Front. Neurosci.* **2023**, *17*, 1087912.
- [19] S. Fu, J. Xu, S. Chang, L. Yang, S. Ling, J. Cai, J. Chen, J. Yuan, Y. Cai, B. Zhang, Z. Huang, K. Yang, W. Sui, L. Xue, Q. Zhao, *EEE Trans. Med. Imaging* **2023**, *43*, 39.
- [20] Y. Tang, F. Xu, P. Lei, G. Li, Z. Tan, *Skin Res. Technol.* **2023**, *29*, e13308.
- [21] P. Hu, B. Niu, H. Yang, Y. Xia, D. Chen, C. Meng, K. Chen, B. Biswal, *Microcirculation* **2022**, *29*, e12783.
- [22] O. Semyachkina-Glushkovskaya, A. Abdurashitov, A. Pavlov, A. Shirokov, N. Navolokin, O. Pavlova, A. Gekalyuk, M. Ulanova, N. Shushunova, A. Bodrova, E. Saranceva, A. Khorovodov, I. Agranovich, V. Fedorova, M. Sagatova, A. E. Shareef, C. Zhang, D. Zhu, V. Tuchin, *Chin. Opt. Lett.* **2017**, *15*, 90002.
- [23] T. Aonishi, R. Maruyama, T. Ito, H. Miyakawa, M. Murayama, K. Ota, *Neurosci. Res.* **2022**, *179*, 51.
- [24] V. Kalchenko, D. Israeli, Y. Kuznetsov, I. Meglinski, A. Harmelin, *J. Biophotonics* **2015**, *8*, 897.
- [25] J. Buijs, J. van der Gucht, J. Sprakel, *Sci. Rep.* **2019**, *9*, 13279.
- [26] A. Brazhe, D. Marsh, N. Holstein-Rathlou, O. Sosnovtseva, *PLoS One* **2014**, *9*, e105879.
- [27] R. Patel, C. Steele, A. Chen, S. Patel, G. Devenyi, J. Germann, C. Tardif, M. Chakravarty, *NeuroImage* **2020**, *207*, 116348.
- [28] V. Kalchenko, A. Sdobnov, I. Meglinski, Y. Kuznetsov, G. Molodij, A. Harmelin, *Photonics* **2019**, *6*, 80.
- [29] V. Kalchenko, N. Madar-Balakirski, I. Meglinski, A. Harmelin, *J. Biophotonics* **2011**, *4*, 645.
- [30] V. Kalchenko, Y. Kuznetsov, D. Preise, I. Meglinski, A. Harmelin, *J. Biomed. Opt.* **2014**, *19*, 60502.
- [31] V. Kalchenko, I. Meglinski, Y. Sdobnov, A. Kuznetsov, A. Harmelin, *J. Biomed. Opt.* **2019**, *24*, 60501.
- [32] J. Schindelin, I. Arganda-Carreras, E. Frise, V. Kaynig, M. Longair, T. Pietzsch, S. Preibisch, C. Rueden, S. Saalfeld, B. Schmid, J. Y. Tinevez, D. J. White, V. Hartenstein, K. Eliceiri, P. Tomancak, A. Cardona, *Nat. Methods* **2012**, *9*, 676.
- [33] A. Konovalov, F. Grebenev, D. Stavtsev, I. Kozlov, V. Gadzhiagaev, G. Piavchenko, D. Telyshev, A. Gerasimenko, I. Meglinski, S. Eliava, S. Zalogin, A. Artemyev, G. Golodnev, T. Shumeiko, *Sci. Rep.* **2024**, *14*, 1735.
- [34] D. A. Boas, A. K. Dunn, *J. Biomed. Opt.* **2010**, *15*, 11109.
- [35] A. Sdobnov, A. Bykov, G. Molodij, V. Kalchenko, T. Jarvinen, A. Popov, K. Kordas, I. Meglinski, *J. Phys. D: Appl. Phys.* **2018**, *51*, 155401.
- [36] F. He, C. Sullender, H. Zhu, M. Williamson, X. Li, Z. Zhao, T. Jones, C. Xie, A. Dunn, L. Luan, *Sci. Adv.* **2020**, *6*, eaba1933.
- [37] M. Moreno-Castillo, R. Meza, J. Romero-Vaca, N. Huidobro, A. Méndez-Fernández, J. Martínez-Castillo, P. Mabil, A. Flores, E. Manjarrez, *Front. Neurosci.* **2020**, *14*, 38.
- [38] R. Rungta, M. Zuend, A. Aydin, É. Martineau, D. Boido, B. Weber, S. Charpak, *Commun. Biol.* **2021**, *4*, 855.
- [39] J. Lee, C. Stile, A. Bice, Z. Rosenthal, P. Yan, A. Snyder, J. O. Lee, A. Bauer, *J. Cereb. Blood Flow Metab.* **2021**, *41*, 841.
- [40] G. Paxinos, K. Franklin, *Paxinos and Franklin's the mouse brain in stereotaxic coordinates*, Academic Press, Amsterdam **2019**.
- [41] J. Bugge, *Acta Anaesthesiol. Scand.* **2009**, *53*, 1239.
- [42] V. Tsytsarev, *Behav. Brain Res.* **2022**, *419*, 113684.
- [43] K. Barksdale, E. Perez-Costas, J. Gandy, M. Melendez-Ferro, R. Roberts, G. Bijur, *FASEB J.* **2010**, *24*, 3590.
- [44] S. Tisherman, *Ann. N. Y. Acad. Sci. U. S. A.* **2022**, *1509*, 5.

AUTHOR BIOGRAPHIES



Anton Sdobnov is a post-doctoral researcher at the Opto-Electronics and Measurement Techniques Unit (OPEM), University of Oulu, Finland. In 2021, Anton received a Ph.D. degree in physics at Saratov State University, Russia. In 2022, he received a D.Sc. degree in technology at the University of Oulu, Finland. His scientific interests are in the areas of non-invasive biomedical imaging, tissue optical clearing, and vortex light propagation in scattering media.



Vassiliy Tsytsarev obtained Ph.D. in neuroscience in Saint-Petersburg State University, Russia. After 7 years work in the Brain Science Institute of RIKEN in Japan he moved to the US and switched to the somatosensory cortex, while maintaining interest in new methods of brain imaging. His current research in the University of Maryland (UMB) is focused on the functional brain mapping, epileptic studies neural network and traumatic brain injury and regeneration, working mainly of the rodent somatosensory system, a perfect object for many types of neuroscience research, including models of neural diseases. He is member of the board of directors of Society for Brain Mapping and Therapeutics (SBMT).



Gennadii Piavchenko received his MD in neurology, Ph.D. in cellular biology, and M.Sc. in pedagogics. He is an associate professor at the Human Anatomy and Histology Department at Sechenov First Moscow State Medical University, Moscow. His research interests primarily revolve around the development and practical implementation of interdisciplinary approaches that integrate behavioral neuroscience and applied pharmacology with emerging trends in biophotonics.



Alexander Bykov is an adjunct professor (Docent) in biophotonics and sensors technologies at the Opto-Electronics and Measurement Techniques Unit (OPEM), University of Oulu, Finland. In 2010, he received his D.Sc. (Tech.) degree. Since 2019, he has been the leader of the Biophotonics Group at OPEM. His scientific interests are in the areas of non-invasive optical diagnostics of biotissues, the theory of light propagation in scattering media, and numerical simulation of light transport. He is a senior member of Optica.



Igor Meglinski is a professor in quantum biophotonics and biomedical engineering at the College of Engineering and Physical Sciences at Aston University (UK). His research interests lie at the interface between physics, optics, and biomedical engineering, focusing on the development of new non-invasive imaging/diagnostic techniques and their application in medicine and biology, pharmacy, environmental monitoring, food sciences and health care industries. He is a chartered physicist (CPhys) and chartered engineer (CEng), senior member of IEEE, fellow of Institute of Physics, FRMS, fellow SPIE, and fellow OPTICA (formerly Optical Society of America).

SUPPORTING INFORMATION

Additional supporting information can be found online in the Supporting Information section at the end of this article.

How to cite this article: A. Sdobnov, V. Tsytsarev, G. Piavchenko, A. Bykov, I. Meglinski, *J. Biophotonics* **2024**, e202400017. <https://doi.org/10.1002/jbio.202400017>